



HAL
open science

Evidential modeling for pose estimation

Fabio Cuzzolin, Ruggero Frezza

► **To cite this version:**

Fabio Cuzzolin, Ruggero Frezza. Evidential modeling for pose estimation. 4th International Symposium on Imprecise Probabilities and Their Applications (ISIPTA'05), Jul 2005, Pittsburgh, United States. inria-00590191

HAL Id: inria-00590191

<https://hal.inria.fr/inria-00590191>

Submitted on 6 May 2011

HAL is a multi-disciplinary open access archive for the deposit and dissemination of scientific research documents, whether they are published or not. The documents may come from teaching and research institutions in France or abroad, or from public or private research centers.

L'archive ouverte pluridisciplinaire **HAL**, est destinée au dépôt et à la diffusion de documents scientifiques de niveau recherche, publiés ou non, émanant des établissements d'enseignement et de recherche français ou étrangers, des laboratoires publics ou privés.

Evidential modeling for pose estimation

Fabio Cuzzolin

UCLA Vision Laboratory
University of California at Los Angeles
cuzzolin@cs.ucla.edu

Ruggero Frezza

Dipartimento di Ingegneria dell'Informazione
Università di Padova
frezza@dei.unipd.it

Abstract

Pose estimation involves reconstructing the configuration of a moving body from images sequences. In this paper we present a general framework for pose estimation of unknown objects based on Shafer's evidential reasoning. During learning an *evidential model* of the object is built, integrating different image features to improve both estimation robustness and precision. All the measurements coming from one or more views are expressed as *belief functions*, and combined through Dempster's rule. The best pose estimate at each time step is then extracted from the resulting belief function by probabilistic approximation. The choice of a sufficiently dense training set is a critical problem. Experimental results concerning a human tracking system are shown.

Keywords. Pose estimation, training set, feature-pose maps, belief functions, evidential model.

1 Introduction

Object tracking [8] is one of the most active field of computer vision, concerning the reconstruction of the actual pose of a moving object by processing the sequence of images taken during its motion. Most of the literature concerns *model-based* approaches [6]. In case of articulated objects composed by a number of rigid parts [2], a popular choice is to use a kinematic model, while when tracking general non-rigid objects one has to recur to flexible models whose parameters are no more in relation with the relative positions of rigid subsets of the body. Statistical estimation methods have been recently introduced, ranging from maximum a-posteriori (MAP) estimation, to applications of particle filtering or multiple hypothesis techniques. All those methods however contemplate the introduction of some kind of model of the moving body, in terms of observation likelihoods, volumetric models, or other.

Consider instead a scenario in which the configuration of an *unknown* object is desired, having no a-priori information about the nature itself of the body (i.e. rigid, articulated, deformable, etc.). As we show in this paper, the only way of doing inference on the object pose is then building a map between some salient image measurements (*features*) and poses through a *learning* procedure.

In a training session the object describes an exciting enough trajectory approximating the actual parameter space \mathcal{Q} : a finite approximation $\tilde{\mathcal{Q}}$ of the parameter space is hence acquired as a collection of poses assumed by the object. These ground truth configuration values can be produced for instance by a motion capture system, as in [11].

At the same time, a number of features are extracted from one or more image sequences. Their ranges (features spaces) are discretized by feeding a *hidden Markov model* (HMM) with the acquired measurements, and the maps from the approximate feature spaces to the approximate configuration space $\tilde{\mathcal{Q}}$ are learned. These maps, together with discrete feature and parameter spaces form the learned *evidential model* of the object: when the object evolves freely, the evidential model can be used to estimate its pose. We propose a cue integration approach based on the theory of evidence [12] in which the uncertainty on the measurements is described through *belief functions* (b.f.), as they have no need for prior distributions (an attractive feature in a model-free estimation process). New features are transformed into belief functions, combined, and then a pointwise estimate of the body pose is computed by probabilistic approximation. Experimental results concerning human body tracking in a challenging situation are presented.

2 Pose estimation

Given an object moving in front of one or more cameras, the *pose estimation* problem consists on estimating at each time instant its configuration or *pose* from

the available images. We assume that the pose of the moving object can be expressed as a point in some region \mathcal{Q} of \mathbb{R}^D , called *parameter space*. In the case of a rigid body (for example, an airplane flying in the field of view of the cameras) the pose is simply the position and orientation of the object with respect to some fixed reference frame (for the plane, 3 coordinates giving its location and other 3 coordinates expressing its motion direction, $D = 6$).

If the body is *articulated* (composed by several rigid bodies) like a human arm or hand, its pose also describes its internal configuration. A common choice is to assume a kinematic model describing the angles between the rigid parts or links forming the object. For instance, Rehg and Kanade [10] used a kinematic model of the hand with $D = 27$ degrees of freedom (see Figure 1) representing the angles between each pair of links of the fingers. As the object evolution

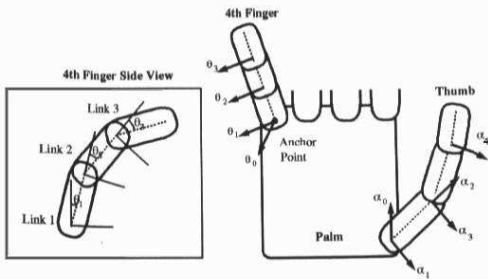


Figure 1: Rehg's kinematic model of the hand.

is observed through one or more cameras, its pose must then be estimated from the available images. However, as images themselves are too large and redundant to be useful, usually a number of salient measurements (*features*) are extracted from them to be used in the estimation process. Rehg, for instance, measured the projected locations of the fingertips of the hand on the image plane.

2.1 Pose estimation of unknown objects

Consider now a situation in which we want to estimate the configuration of an unknown object, having no model or a-priori information about the nature of the body itself (i.e. rigid, articulated, deformable, etc.). The only way of estimating the object pose is then building a *map between features and poses*, which would allow us to make inference on the pose $q \in \mathcal{Q}$ given the evidence extracted from the images. As we have no knowledge of the analytic relations between image features and body configurations, this has to be done directly from the data by means of a *learning* strategy. In a training session the object evolves, exploring its range of possible configurations, and a set

of its poses is collected to form a finite approximation $\tilde{\mathcal{Q}}$ of the parameter space

$$\tilde{\mathcal{Q}} \doteq \{q_k, k = 1, \dots, T\}. \quad (1)$$

At the same time a number N of features

$$\{y_i(k), k = 1, \dots, T\}, \quad i = 1, \dots, N \quad (2)$$

are extracted from the images at each time instant k . As they are collected by cameras at a finite, constant pace, the number of feature measurements is finite.

To collect $\tilde{\mathcal{Q}}$ we need a source of “ground truth” telling us what the object pose is at each instant k of the training session. One possibility is using a motion capture system as done in [11] or [7] for the human body tracking problem. In particular, if we apply a number of reflective markers in fixed positions of the body, the system is able to provide (through some triangulation algorithm) the 3D locations of the markers during the motion in the training stage. Since we do not know the parameter space of the object, it is reasonable to adopt the markers’ locations as body configuration. This way the motion capture system generates the desired sequence of poses (1).

Ideally, $\tilde{\mathcal{Q}}$ should be somehow “dense” in \mathcal{Q} : $\forall q \in \mathcal{Q}$ there should be a sample q_k such that $\|q - q_k\| < \epsilon$ for some ϵ small enough. Clearly as the actual shape of the parameter space is unknown such a condition is hard to impose.

Given the training data (1), (2), *hidden Markov models* provide a method to automatically build feature-pose maps that can eventually be used for model-free pose estimation.

3 Feature-pose maps

A hidden Markov model is a finite state stochastic model in which the states $\{X_k\}$ form a *Markov chain*; the only observable quantity is a corrupted version Y_k of the state called *observation process*. We can associate the elements of the finite state space $\mathcal{X} = \{1, \dots, n\}$ to coordinate versors $e_i = (0, \dots, 0, 1, 0, \dots, 0) \in \mathbb{R}^n$ and write the model as [9]

$$\begin{cases} X_{k+1} = AX_k + V_{k+1} \\ Y_{k+1} = CX_k + \text{diag}(W_{k+1})\Sigma X_k \end{cases}$$

where $\{V_{k+1}\}$ is a sequence of martingale increments and $\{W_{k+1}\}$ is a sequence of i.i.d. Gaussian noises $\mathcal{N}(0, 1)$. The HMM parameters are the *transition matrix* $A = (a_{ij}) = P(X_{k+1} = e_i | X_k = e_j)$, the matrix C collecting the means of the state-output distributions (as the j -th column C_j of C is equal to $E[p(Y_{k+1} | X_k = e_j)]$), and the matrix Σ of the variances of the output distributions.

3.1 Approximate feature spaces

A, C and Σ can be estimated, given a sequence of observations (the feature sequence in our case) through the *Expectation-Maximization* (EM) algorithm. Also, when applied to a sequence of feature values $\{y_i(k), k = 1, \dots, T\}$ acquired in the training session, the EM algorithm provides a multi-modal Gaussian approximation of the original feature space (the range $\mathcal{Y}_i \subset \mathbb{R}^{d_i}$ of the unknown feature function $y_i : \mathcal{I} \rightarrow \mathcal{Y}_i$ on the set of all images \mathcal{I}). More

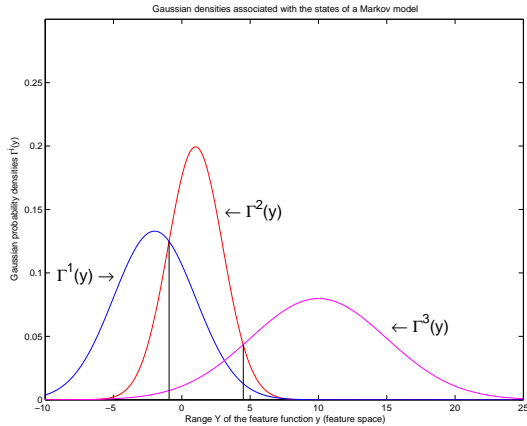


Figure 2: Implicit partition associated with a Markov model with three states. To each state corresponds a Gaussian density on the range \mathcal{Y} of the feature function (abscissa). Together they detect a partition of the range into three regions $\mathcal{Y}^1, \mathcal{Y}^2, \mathcal{Y}^3$ (separated by the vertical lines).

precisely, a set of n_i Gaussian densities (one for each state) $\{\Gamma_i^j, j = 1, \dots, n_i\}$ on the i -th feature space is set up: their means and variances are collected in C and Σ , respectively. This is equivalent to an *implicit* partition

$$\Pi_{\mathcal{Y}_i} = \{\mathcal{Y}_i^1, \dots, \mathcal{Y}_i^{n_i}\} \quad (3)$$

of the feature range (see Figure 2), where $\mathcal{Y}_i^j = \{y \in \mathcal{Y}_i \text{ s.t. } \Gamma_i^j(y) > \Gamma_i^l(y) \forall l \neq j\}$.

The collection (3) is a finite representation of the range of the i -th feature function: we call it *approximate* feature space.

3.2 Learning feature-parameter maps

As a consequence, for each feature i each sample pose q_k in the training set $\tilde{\mathcal{Q}} = \{q_k, k = 1, \dots, T\}$ is mapped to the element \mathcal{Y}_i^j of the implicit partition (3) such that $y_i(k) \in \mathcal{Y}_i^j$

$$\forall i, k \quad q_k \mapsto \mathcal{Y}_i^j : y_i(k) \in \mathcal{Y}_i^j.$$

On the other hand, each element \mathcal{Y}_i^j of the discrete feature space is mapped to the set of training poses whose feature value fall in \mathcal{Y}_i^j ,

$$\omega_i : \mathcal{Y}_i^j \mapsto \tilde{\mathcal{Q}}_i^j \doteq \{q_k \in \tilde{\mathcal{Q}} : y_i(k) \in \mathcal{Y}_i^j\}. \quad (4)$$

The application of the EM algorithm to all the feature sequences (2) then yields N maps (4) from each approximate feature space (3) to the approximate parameter space $\tilde{\mathcal{Q}}$.

4 Evidential modeling

Once feature-pose maps are learnt from the training data they can be used to design a method for estimating the pose of the object of interest. As single features cannot guarantee of stability and invariance to nuisance factors, extracting multiple cues can be useful to solve ambiguities and increase the robustness of the overall system. Some researchers have actually posed the cue integration issue in a rigorous probabilistic setup [16]. However, in a Bayesian setting it is hard to design a model-independent feature extraction process, and a number of independence or incorrelation assumptions are needed to make the formulas tractable [14].

4.1 The theory of evidence

We propose an uncertainty description based on *theory of evidence* as, in contrast to the Bayesian formalism, *no a-priori distributions are needed* [12] as required in the model-free estimation problem introduced in Section 2.

Definition 1. A basic probability assignment (*b.p.a.*) on a finite set (*FOD*) Θ is a function $m : 2^\Theta \rightarrow [0, 1]$ such that $m(\emptyset) = 0$, $m(A) \geq 0 \forall A \subset \Theta$, $\sum_{A \subset \Theta} m(A) = 1$.

2^Θ denotes the power set of Θ . The elements of 2^Θ associated with non-zero values of m are called *focal elements* (f.e.) and their union \mathcal{C} *core*.

Definition 2. The belief function s associated with a basic probability assignment m is the unique function $s : 2^\Theta \rightarrow [0, 1]$ such that $s(A) = \sum_{B \subset A} m(B)$.

In the theory of evidence finite probability functions are just peculiar belief functions such that $m(A) = 0 \forall A \text{ s.t. } |A| > 1$ (*Bayesian* b.f.). Belief functions can be combined by means of Dempster's rule.

Definition 3. The orthogonal sum or Dempster's sum of two belief functions s_1, s_2 is a new belief function $s_1 \oplus s_2$ whose focal elements are all the possible non-empty intersections between focal elements A_i, B_j

of s_1 and s_2 respectively, and whose b.p.a. is given by

$$m(A) = \frac{\sum_{i,j:A_i \cap B_j = A} m_1(A_i) \cdot m_2(B_j)}{1 - \sum_{i,j:A_i \cap B_j = \emptyset} m_1(A_i) \cdot m_2(B_j)}. \quad (5)$$

The theory’s major restriction (at least in its original formulation ¹) is the fact that belief functions are defined on finite domains. However, as the training set $\tilde{\mathcal{Q}}$ is finite, the use of belief functions is not problematic.

4.2 Evidential model

Dense training sets (as defined in Section 2.1) are good formal approximations of the unknown parameter space of the moving object. On their side, HMMs provide a method for finding multi-modal approximations of the involved feature spaces, and a way of building maps from each feature space to the approximate parameter space. A unifying framework in which to arrange training sets, approximate feature spaces and feature-pose maps would be desirable. The theory of evidence is such a framework, as both approximate feature spaces (3) and training sets (1) can be thought of as FODs. We will denote with $\Theta_i = \{\theta_i^1, \dots, \theta_i^{n_i}\}$ the FOD corresponding to the implicit partition Π_{y_i} .

For each feature i , the collection $\pi_i^{\tilde{\mathcal{Q}}} \doteq \{\tilde{\mathcal{Q}}_i^j, j = 1, \dots, n_i\}$ forms a partition of the approximate parameter space $\tilde{\mathcal{Q}}$. In the evidential language the EM algorithm builds a *refining* ω_i (4) between each approximate feature space (3) and the training set $\tilde{\mathcal{Q}}$.

Definition 4. Given two FODs Θ and Ω , a map $\omega : 2^\Theta \rightarrow 2^\Omega$ is called *refining* if it satisfies the following conditions: 1) $\omega(\{\theta\}) \neq \emptyset \forall \theta \in \Theta$; 2) $\omega(\{\theta\}) \cap \omega(\{\theta'\}) = \emptyset$ if $\theta \neq \theta'$; 3) $\bigcup_{\theta \in \Theta} \omega(\{\theta\}) = \Omega$.

A refining ω maps Θ to a disjoint partition of Ω . Ω is called a *refinement* of Θ , while Θ is said a *coarsening* of Ω (see Figure 3-top)).

As a map between features and configurations, a refining ω_i allows us to make inferences in $\tilde{\mathcal{Q}}$ on the pose of the moving object, based on the evidence provided by a feature measurement living in Θ_i . However, as inferences based on a single feature are often inaccurate and unreliable, we select in the training stage a number of different features and build a refining for each of them.

$\tilde{\mathcal{Q}}$ then becomes the *common refinement* [12] of the collection of approximate feature spaces $\Theta_1, \dots, \Theta_N$ (Figure 3-bottom), and is the place where all the evidence provided by the different image measurements

¹In fact Shafer extended the theory to infinite frames of discernment in [13].

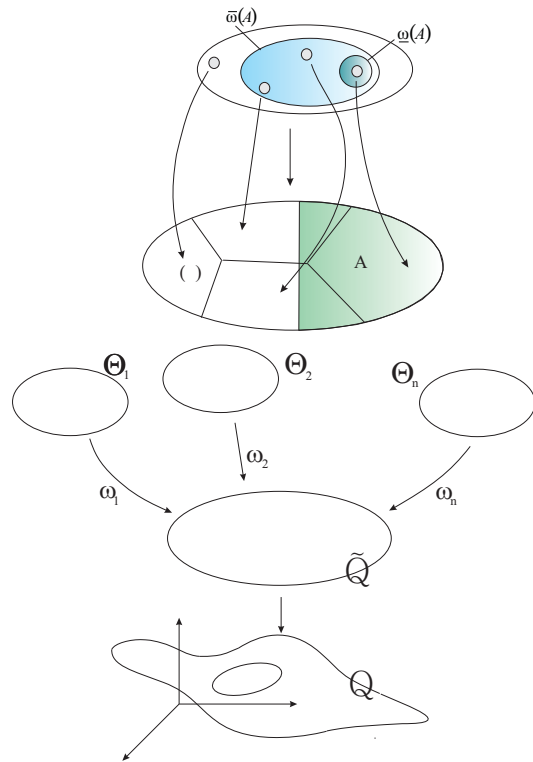


Figure 3: (top) A refining ω between two FODs Θ and Ω . Each element $\theta \in \Theta$ is associated with an element of a disjoint partition of Ω . Each subset $A \subset \Omega$ can be mapped to its inner $\omega(A)$ or $\bar{\omega}(A)$ outer reduction as in figure. (bottom) Evidential model architecture.

y_1, \dots, y_N can be combined. As we will see in Section 5, this can be done by representing features as belief functions and projecting them on the approximate parameter space by means of the refinings learnt in the training stage.

The collection of FODs $\tilde{\mathcal{Q}}, \Theta_1, \dots, \Theta_N$ along with their refining maps is characteristic of both the unknown object to track and the chosen feature functions y_1, \dots, y_N : we call it *evidential model*.

5 Pose estimation

5.1 Measurement functions

The evidential model of the object is built in the training stage, when an adequate training set of the object’s motion is acquired (see Section 2.1). After that, it can be used to estimate the pose of the moving object, as new evidence becomes available.

When a new image is acquired, new visual features are extracted. Those continuous features can be transformed into belief functions on the approximate feature spaces: $y_i \mapsto s_i : 2^{\Theta_i} \rightarrow [0, 1]$. We call these b.f.

measurement functions (m.f.).

This can be done in two steps. Given as input a feature value $y_i \in \mathcal{Y}_i$ the Markov model \mathcal{H}_i produces as output the set of *likelihoods* $\{\Gamma_i^j(y_i), j = 1, \dots, n_i\}$ of this measurement with respect to each state e_j of the model (see Figure 2). Computing the measurement function s_i then reduces to building a belief function from this set of likelihoods. These in turn detect a *consonant* belief function (i.e. a b.f. whose focal elements are *nested*, [12]) through the following expression, due to Shafer:

$$s_i(A) = 1 - \frac{\max_{\theta_i^j \in \bar{A}} \Gamma_i^j(y_i)}{\max_{\theta_i^j \in \Theta_i} \Gamma_i^j(y_i)}.$$

The consonant measurement functions s_1, \dots, s_N have then to be projected to the common refinement $\tilde{\mathcal{Q}}$ to be combined, in order to infer the current pose \hat{q} of the object.

5.2 Projections of measurement functions

In model-free estimation it is hard to formulate analytic relations between distinct features as they may concern completely unrelated aspects of the images. The evidential model, instead, provides a formal description of these relations in terms of refinings.

Definition 5. *The maps $\underline{\omega} : 2^\Omega \rightarrow 2^\Theta$, $\underline{\omega}(A) = \{\theta \in \Theta | \omega(\{\theta\}) \subset A\}$ and $\bar{\omega} : 2^\Omega \rightarrow 2^\Theta$, $\bar{\omega}(A) = \{\theta \in \Theta | \omega(\{\theta\}) \cap A \neq \emptyset\}$ are called inner and outer reduction associated with the refining ω .*

Roughly speaking, $\underline{\omega}(A)$ is the largest subset of Θ that implies A, while $\bar{\omega}(A)$ is the smallest subset of Θ implied by A (see Figure 3-top again).

If Ω is a refinement of Θ with refining ω then a b.f. $s' : 2^\Omega \rightarrow [0, 1]$ on Ω is called the *vacuous extension* of a b.f. $s : 2^\Theta \rightarrow [0, 1]$ on Θ iff $s(A) = s'(\omega(A))$ for all $A \subset \Theta$, and its focal elements are exactly the images of focal elements of s : $m'(B) \neq 0$ iff $B = \omega(A)$ for some A s.t. $m(A) \neq 0$.

Every m.f. then generates a collection of “sister” functions defined on the other FODs, called *projections*.

Theorem 1. *The projection of a m.f. s_i defined on Θ_i onto another discrete feature space Θ_j has the following expression: $\pi_j[s_i] : 2^{\Theta_j} \rightarrow [0, 1]$, $\pi_j[s_i] = s_i \circ \underline{\omega}_i \circ \omega_j$. Its basic probability assignment can be computed from m_i as $\pi_j[m_i](A) = \sum_{B \subset \Theta_i: \bar{\omega}_j(\omega_i(B))=A} m_i(B)$.*

Proof. The vacuous extension s' of a belief function $s : 2^\Theta \rightarrow [0, 1]$ to a refinement Ω , $\omega : 2^\Theta \rightarrow 2^\Omega$ has a b.p.a. m such that $m(A) = m'(\omega(A)) = m' \circ \omega$ and can be expressed as $s' = s \circ \underline{\omega}$ ([12], Theorem 7.4). The

projection $\pi_j[s_i]$ of a b.f. $s_i : 2^{\Theta_i} \rightarrow [0, 1]$ onto another discrete feature space Θ_j is then the restriction to Θ_j of the vacuous extension of s_i to $\tilde{\mathcal{Q}}$, so that $\pi_j[s_i] = s'_j \circ \omega_j = s_i \circ \underline{\omega}_i \circ \omega_j$. Its basic probability assignment is $\pi_j[m_i](A) = \sum_{C \subset \tilde{\mathcal{Q}}: \bar{\omega}_j(C)=A} m'_i(C)$ which is equal to

$$\sum_{B \subset \Theta_i: \bar{\omega}_j(\omega_i(B))=A} m'_i(\omega_i(B)) = \sum_{B \subset \Theta_i: \bar{\omega}_j(\omega_i(B))=A} m_i(B)$$

for $m'_i(C) \neq 0$ iff C is the image of a f.e. B of s_i . \square

As a consequence, the set of focal elements of $\pi_j[s_i]$ is $\mathcal{E}_{\pi_j[s_i]} = \{A \subset \Theta_j | A = \bar{\omega}_j(\omega_i(B)), B \in \mathcal{E}_{s_i}\}$ and its core $\mathcal{C}_{\pi_j[s_i]} = \bar{\omega}_j(\omega_i(\mathcal{C}_{s_i}))$.

Theorem 2. *The projection of a consonant belief function is still consonant, even if it has not in general the same number of focal elements.*

Proof. Let us call $\mathcal{A}_1 \subseteq \dots \subseteq \mathcal{A}_K$ the nested focal elements of s : obviously its extension s' to $\tilde{\mathcal{Q}}$ has as focal elements $\omega_i(\mathcal{A}_1), \dots, \omega_i(\mathcal{A}_K)$. They are all distinct subsets of $\tilde{\mathcal{Q}}$ for ω is a refining. They are also nested so that s' is still a consonant b.f. over $\tilde{\mathcal{Q}}$. Now, the focal elements of $\pi_j[s_i]$ are the restrictions of those subsets to Θ_j :

$$\bar{\omega}_j(\omega_i(\mathcal{A}_k)) = \{\theta \in \Theta_j | \omega_j(\{\theta\}) \cap \omega_i(\mathcal{A}_k) \neq \emptyset\}.$$

Since they are nested, if $\omega_j(\{\theta\}) \cap \omega_i(\mathcal{A}_k) \neq \emptyset$ then $\omega_j(\{\theta\}) \cap \omega_i(\mathcal{A}_l) \neq \emptyset$, $l \geq k$ so that $\bar{\omega}_j(\omega_i(\mathcal{A}_k)) \subset \bar{\omega}_j(\omega_i(\mathcal{A}_l))$, $l \geq k$ i.e. $\pi_j[s_i]$ is consonant. However, it is not generally true that $\forall k, l \exists \theta \in \Theta_j$ s.t. $\theta \in \bar{\omega}_j(\omega_i(\mathcal{A}_l))$ and $\theta \notin \bar{\omega}_j(\omega_i(\mathcal{A}_k))$: it is actually easy to find a counterexample. Hence in the chain $\bar{\omega}_j(\omega_i(\mathcal{A}_1)) \subset \dots \subset \bar{\omega}_j(\omega_i(\mathcal{A}_K))$ some equalities may appear. \square

Theorem 2 shows how consonant belief functions are then *invariant under projection*, and hence a formally correct representation of feature measurements.

5.3 Pointwise estimation

Once the measurement functions s_1, \dots, s_N are projected onto $\tilde{\mathcal{Q}}$, they can be combined using Dempster’s rule. In absence of conflict the orthogonal sum of the m.f. finally yields a belief function \hat{s} on $\tilde{\mathcal{Q}}$. The easier way to extract a single pose estimate \hat{q} from the belief estimate is then approximating \hat{s} with a finite probability \hat{p} on $\tilde{\mathcal{Q}}$, and then compute its mean value

$$\hat{q} = \sum_{k=1}^T \hat{p}(q_k) \cdot q_k.$$

The problem of approximating a belief function with a finite probability has been widely studied [3, 18].

Natural approximations of a belief function s are the relative plausibility of singletons $\hat{p} = \tilde{P}_s^*$ [17]

$$\tilde{P}_s^*(\theta) = \frac{P_s^*(\{\theta\})}{\sum_{\theta' \in \Theta} P_s^*(\{\theta'\})}$$

where $P_s^* : 2^\Theta \rightarrow [0, 1]$ is the associated plausibility function, or the pignistic function [15]. Under weak local linearity assumptions on the parameter space, this approximation produces good results.

Several fast implementation of Dempster's rule exist for restricted situations (see [1, 5] among the others). However, consonant b.f. can only have n focal elements (being nested, Section 5.1). This reduces the computational complexity of their sum to $O(n^2)$ instead of $O(2^{2n})$.

6 Analysis of the evidential model

6.1 Quantization and ambiguities

We have seen that learning a model directly from the data necessarily implies some sort of approximation of the involved spaces in terms of samples. However, this has non-trivial consequences on the performance of the resulting estimation. In particular, the degree of discretization of feature spaces and training set have a direct influence on the presence of ambiguities during estimation.

Again, the evidential formalism is powerful enough to give a formal picture of the ambiguity issue, and help the assessment of the adequate level of quantization. We have seen how \tilde{Q} is a common refinement of the approximate feature spaces. However, a collection of compatible FODs has many common refinements. One of these is particularly simple.

Definition 6. Consider a collection of compatible FODs $\Theta_1, \dots, \Theta_N$. If another FOD Θ is such that: 1) $\forall i \exists \omega_i : 2^{\Theta_i} \rightarrow 2^\Theta$ refining; 2) $\forall \theta \in \Theta \exists \theta_i \in \Theta_i$ for all $i = 1, \dots, N$ such that $\{\theta\} = \omega_1(\{\theta_1\}) \cap \dots \cap \omega_N(\{\theta_N\})$, then this unique [12] FOD $\Theta \doteq \Theta_1 \otimes \dots \otimes \Theta_N$ is called minimal refinement of the collection $\Theta_1, \dots, \Theta_N$.

$\Theta_1, \dots, \Theta_N$ are said to be *independent* if $\omega_1(A_1) \cap \dots \cap \omega_N(A_N) \neq \emptyset$ whenever $\emptyset \neq A_i \subset \Theta_i \forall i$.

Now, imagine that the N feature functions assume the discrete values $\theta^1, \dots, \theta^N$ respectively. Each piece of evidence implies an object pose inside the subset $\omega_i(\theta^i)$ of the training set, so that from $\theta^1, \dots, \theta^N$ it can be inferred that the estimated pose falls inside the set

$$\omega_1(\theta^1) \cap \dots \cap \omega_N(\theta^N). \quad (6)$$

In other words, configurations in the same intersection of the form (6) are indistinguishable. But now, those subsets *are* the elements of the minimal refinement, so that

Theorem 3. Each pair of poses of the training set can be distinguished under the evidential model iff \tilde{Q} is the minimal refinement of the feature spaces.

In this case, for each training pose q_k there exists a combination of feature values $\theta^1, \dots, \theta^N$ s.t. q_k is perfectly resolved: $q_k = \omega_1(\theta^1) \cap \dots \cap \omega_N(\theta^N)$.

Given a training set it is hence desirable to choose the number of states of the N HMMs associated with each feature space in order to bring the minimal refinement $\Theta_1 \otimes \dots \otimes \Theta_N$ as close as possible to \tilde{Q} . As the ‘‘natural’’ number of states is determined by the clusters actually formed by the feature data acquired in the training session, sometimes the addition of new features becomes necessary to resolve the ambiguities.

6.2 Conflict management

Dempster's combinations of generic belief functions defined on different frames $\Theta_1, \dots, \Theta_N$ are always guaranteed to exist only if $\Theta_1, \dots, \Theta_N$ are *independent* [4]. This could seem a serious obstacle to evidence combination in the evidential model. However, measurement functions are not generic b.f., as they are peculiar b.f. built by means of a HMM (see Section 5.1).

Let us first suppose one of the sample poses q_k is presented to the model, with feature values $y_1(k), \dots, y_N(k)$. In the worst case, for each feature i there will be a single state j_i with $\Gamma_i^{j_i}(y_i) \gg \Gamma_i^j(y_i) \forall l \neq j_i$. The algorithm of Section 5.1 will then yield a set of N Bayesian b.f. with $m_i(\theta_i^{j_i}) = 1, m_i(A) = 0$ for $A \neq \{\theta_i^{j_i}\}$. Now, as $q_k \in \omega_i(\theta_i^{j_i})$ for all i (by definition of ω_i), $\omega_1(\theta_1^{j_1}) \cap \dots \cap \omega_N(\theta_N^{j_N}) \supset q_k \neq \emptyset$ and their Dempster's sum always exists. Hence, a conflict is possible only if $q \notin \tilde{Q}$.

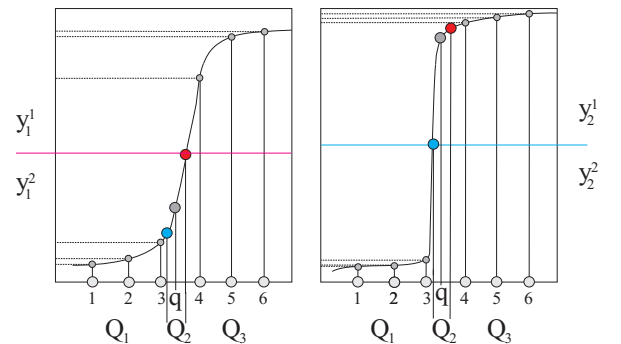


Figure 4: Conflict in the evidential model.

Consider then two scalar features as in Figure 4, with ranges partitioned in 2 clusters delimited by the horizontal lines and a training set formed by the 6 points marked on the absciss. The refining maps are $\omega_1(\mathcal{Y}_1^1) = \{4, 5, 6\}$, $\omega_1(\mathcal{Y}_1^2) = \{1, 2, 3\}$ and $\omega_2(\mathcal{Y}_2^1) =$

$\{4, 5, 6\}$, $\omega_2(\mathcal{Y}_2^2) = \{1, 2, 3\}$ respectively. But now, for each of the poses q in the highlighted region \mathcal{Q}_2 , $\omega_1(y_1(q)) = \{1, 2, 3\}$ while $\omega_2(y_2(q)) = \{4, 5, 6\}$ so that $\omega_1(y_1(q)) \cap \omega_2(y_2(q)) = \emptyset$ and there is no combination.

Formally, each implicit partition of a feature range \mathcal{Y}_i is naturally associated with a partition of the parameter space \mathcal{Q} through the inverse feature map

$$\{\mathcal{Y}_i^1, \dots, \mathcal{Y}_i^{n_i}\} \xrightarrow{y_i^{-1}} \Pi_{\mathcal{Q}}^i = \{y_i^{-1}(\mathcal{Y}_i^1), \dots, y_i^{-1}(\mathcal{Y}_i^{n_i})\}. \quad (7)$$

On the other side, there exists a refining ω'_i between Θ_i and \mathcal{Y}_i , namely $\omega'_i(\theta_i^j) = \mathcal{Y}_i^j$, so that each feature value y_i can be mapped to a set of training poses in $\tilde{\mathcal{Q}}$, $y_i \mapsto \omega_i(\bar{\omega}'_i(y_i)) = \{q_k \in \tilde{\mathcal{Q}} : y_i(q_k) \in \mathcal{Y}_i^{j_{y_i}}\}$ where $\bar{\omega}'_i$ is the reduction of ω'_i and $\mathcal{Y}_i^{j_{y_i}}$ is the region of \mathcal{Y}_i containing y_i . Hence, each object configuration $q \in \mathcal{Q}$ has a set of *representatives* in $\tilde{\mathcal{Q}}$,

$$\omega_1(\bar{\omega}'_1(y_1(q))) \cap \dots \cap \omega_N(\bar{\omega}'_N(y_N(q))). \quad (8)$$

As the above example explains,

Proposition 1. *There is conflict between measurement functions iff the underlying object pose q has no representatives (8) in the training set.*

The intersection of the partitions $\Pi_{\mathcal{Q}}^i$ of the parameter space associated with the quantized feature ranges (Equation (7)) finally detects another partition of \mathcal{Q} ,

$$\Pi_{\mathcal{Q}} = \{y_1^{-1}(\mathcal{Y}_1^{j_1}) \cap \dots \cap y_N^{-1}(\mathcal{Y}_N^{j_N})\}$$

$\forall j_1 = 1, \dots, n_1, \dots, j_N = 1, \dots, n_N$. The non-represented region of \mathcal{Q} is then the set of the elements of $\Pi_{\mathcal{Q}}$ which do not contain any sample pose (as the marked region \mathcal{Q}_2 in Figure 4). This suggests that

Proposition 2. *Conflict is impossible in the evidential model iff $\Pi_{\mathcal{Q}} \sim \Theta_1 \otimes \dots \otimes \Theta_N$.*

Adding new samples in each of the non-represented elements of $\Pi_{\mathcal{Q}}$ (like $q \in \mathcal{Q}_2$ in Figure 4) would ideally solve the problem. Unfortunately, as we have no a-priori knowledge about the parameter space, the best we can do is updating the evidential model each time a conflict takes place, progressively reducing the chance of this happening again.

7 Algorithms

It is time to summarize the learning and estimation algorithms we introduced in Sections 3, 4 and 5.

7.1 Model learning

In the training stage an evidential model of the object is built. The body moves in front of the camera(s),

exploring its parameter space, while a sequence of training poses $\tilde{\mathcal{Q}} = \{q_k, k = 1, \dots, T\}$ is provided by a source of ground truth (for instance a motion capture system, Section 2.1). At the same time:

1. we compute a number of feature measurements y_i , $i = 1, \dots, N$ from all the images;
2. we process every feature sequence $\{y_i(k), k = 1, \dots, T\}$ by means of a HMM \mathcal{H}_i with n_i states, obtaining

2.a the N approximate feature spaces Θ_i , i.e. the implicit partitions of the ranges associated with the states of the corresponding HMMs (Section 3.1);

2.b the N refinings ω_i (4) between each feature space Θ_i and the approximate parameter space $\tilde{\mathcal{Q}}$.

Even after choosing the desired feature functions, the resulting evidential model still depends on the dimensions $\{n_i, i = 1, \dots, N\}$ of the approximate feature spaces (the number of states of the HMMs). The “best” value of n_i can be estimated by analyzing the clusters formed by the training data, or alternatively learned by measuring the estimation error as n_i increases.

7.2 Pose estimation

Given an evidential model of the moving body with N features, estimating the object’s pose reduces to the following steps: Given one or more images at time t

1. the N feature values are extracted from the acquired image(s);
2. the likelihoods $\{\Gamma_i^j(y_i(t)), j = 1, \dots, n_i\}$ of each feature value $y_i(t)$ associated with the corresponding HMM \mathcal{H}_i are computed (Section 3.1);
3. for each feature i a measurement belief function $s_i(t)$ is built from these likelihoods (Section 5.1);
4. all the m.f. $\{s_i(t), i = 1, \dots, N\}$ are projected onto the approximate parameter space $\tilde{\mathcal{Q}}$ by vacuous extension (Section 5.2);
5. in absence of conflict their orthogonal sum $\hat{s}(t) \doteq s_1(t) \oplus \dots \oplus s_N(t)$ is obtained through Dempster’s rule; otherwise the new pose is added to $\tilde{\mathcal{Q}}$, and the model is updated;
6. the pointwise estimate $\hat{q}(t)$ of the object configuration is obtained from $\hat{s}(t)$ after Bayesian approximation (Section 5.3).

8 Experimental results

We tested our evidential modeling technique in a challenging setup, involving the pose estimation of hu-

man arms and legs from two well separated views. To collect the necessary ground truth we used a marker-based motion capture system [11, 7] built by E-motion. The person was filmed by two DV cameras (Figure 5). In the first experiment we asked him to

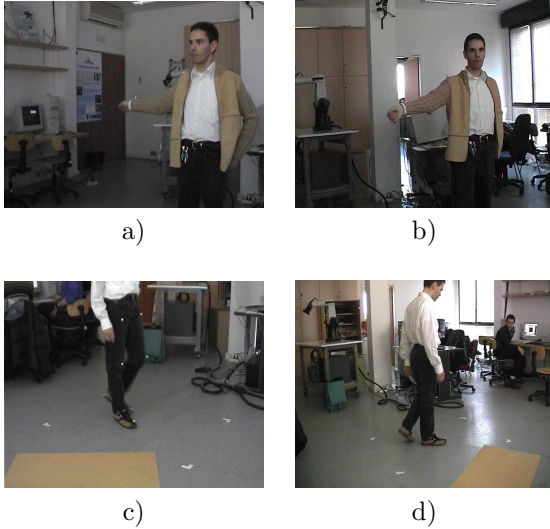


Figure 5: Human bodypart tracking. a),b) Training images of a person moving his right arm. c),d) Training images of the person walking inside a rectangle drawn on the floor.

make his arm follow a trajectory which could hopefully cover the configuration space of the arm itself, keeping his wrist blocked and standing on a fixed spot on the floor to reduce the dimensionality of the space (2 d.o.f.s for the shoulder and 2 for the elbow). In the second experiment we tracked the legs, assuming that the person was walking normally on the floor, and collected the training set by sampling a random walk on a small part of the floor.

We adopted color segmentation to separate the moving object from a non-static background through a colorimetric analysis of the body of interest (Figure 6). We then found the bounding box around the the silhouette of the segmented upper torso or legs, building a feature vector as the collection $\max(row)$, $\min(row)$, $\max(col)$, $\min(col)$ of the row and column indexes defining the box. For the arm experiment we placed four markers on shoulder, elbow, wrist and hand, and used the resulting 12-component vector of their 3D positions as body pose. For the leg experiment we placed 6 markers on hips, knees and feet. The length of the training sequences was 1726 frames for the arm and 1952 frames for the legs. We then built for the arm experiment *three* different evidential models: one using the left view only, with $N = 2$ feature spaces and $n_i = 5$ states for both features; a second model for the right view only, with $N = 3$

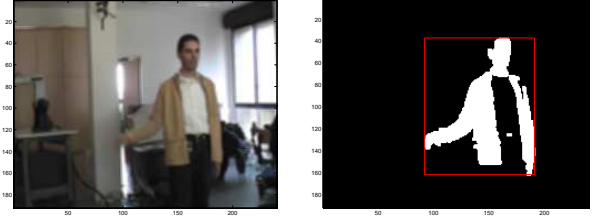


Figure 6: Feature extraction process. Left: original image. Right: the object of interest is color segmented, and the bounding box around it is detected.

and $n_i = const = 5$; an overall model in which all the features from both view were integrated. For the leg experiment we instead built two models with $N = 6$ and $n = 4$ or $n = 5$ respectively to investigate the influence of the quantization level. We

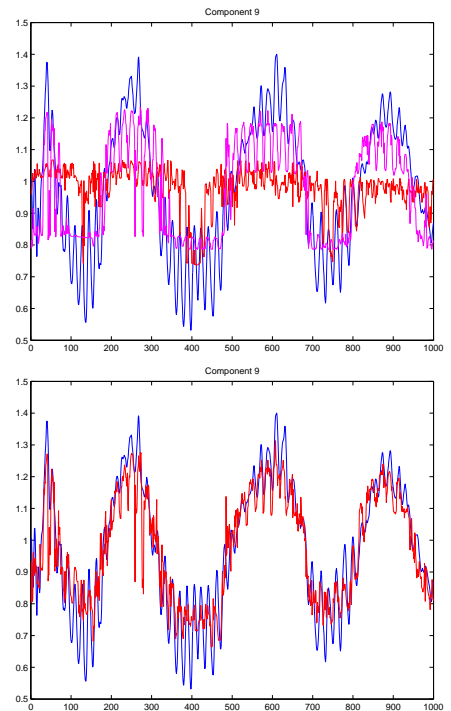


Figure 7: Left: pose estimates of the ninth component of the configuration vector (Y coordinate of the hand marker) produced by the left (red) and right (magenta) model compared to the ground truth (blue), plotted against time. Right: the estimate sequence (red) yielded by the overall model compared to the ground truth.

acquired a testing sequence for each experiment and compared the results with the ground truth provided by the E-motion system. The single-view estimates were rather mediocre. Accordingly, the minimal refinements $\otimes \Theta_i$ for the left and right models were of

size 22 and 80 respectively (the larger the size, the finer the resolution of the model).

As Figure 7 shows, the estimates obtained exploiting both views were clearly better than a simple selection of the best partial estimate at each instant, as the ambiguity analysis confirms. $\otimes \Theta_i$ for the overall model had size 372 and the sizes of the five largest undistinguished regions of \mathcal{Q} were 69,53,43,38,28 respectively, with 139 samples perfectly resolved!

We also computed the estimation error by measuring the Euclidean distance between the real and estimated 3D location of each marker over the whole testing sequence. The average estimation errors were 17.3, 7.95, 13.03, and 2.7 centimeters respectively for the four markers.

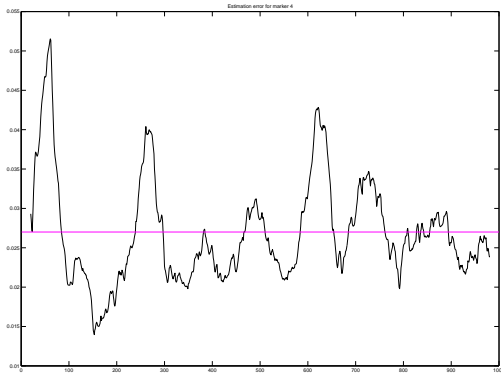


Figure 8: Estimation errors for markers 4 in the arm experiment. The horizontal line indicates the average value.

Figure 9 shows instead the performance of the estimation algorithm in the leg experiment, for a 200-frame-long test sequence. The results were a bit less impressive but still good, mainly due to the difficulty of segmenting a pair of black pants against a dark background (see Figure 5c). This is confirmed by the numerical results. The average estimation errors were 25.41, 19.29, 21.84, 19.88, 23.00, and 22.71 centimeters respectively. Consider that the cameras were located at a distance of about three meters. No significant conflict problem was reported.

8.1 Other learning-based approaches

A comparison with the performance of other methods only makes sense for data-driven model building methods. In fact, a small number of other researchers have proposed an estimation framework based a learning process. Howe *et al.* [7] proposed to use some a-priori knowledge about human motion learned from

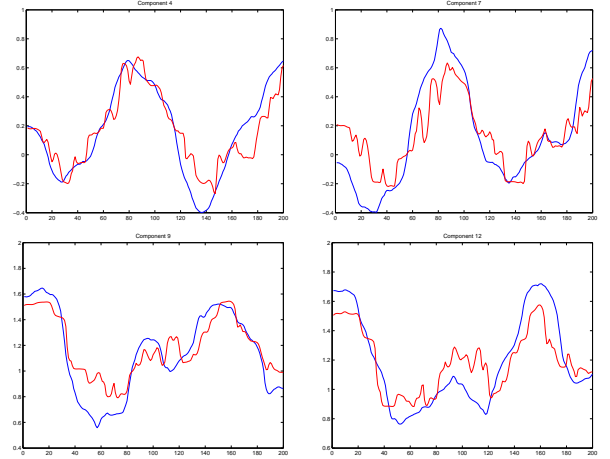


Figure 9: Performance of the two-view pose estimation for the leg experiment on a testing sequence of length 200 with $N = 6$ and $n_i = n = 5$. The estimates for some significant components of the pose vector (components 4,7,9, and 12) are shown in red, against the ground truth values (in blue).

training data to resolve the ambiguities of monocular tracking. They modeled the probabilities of short motions called *snippets* as a mixture of Gaussian density, and adopted EM to find the weight of each cluster. However, the system was tested on short clips only, as the authors admitted it would not be reliable for significantly long sequences. Here instead we have tested our algorithms over rather long sequences.

Rosales and Sclaroff [11] proposed instead a pose estimation technique in which the object pose was expressed as a 2D marker configuration. In the training stage, a motion capture system provided the 3D marker positions of the given object in the motion sequences, whose 2D projections formed the ground truth of the learning process. A 3D model of the object was then used to generate synthetic silhouette views, from which some visual features were extracted. The training set of projected 2D markers was clustered using the EM algorithm, and for each cluster a multi-layer perceptron was trained to map features to 2D marker positions, analogously to what we have shown in Section 3.2.

The training data was more extensive, consisting on 5 sequences of some 200 frames each. The method was applied to synthetic silhouettes obtained through a 3D model, while the results seemed to degrade a little when real video data were considered.

9 Conclusions

In this paper we presented a bottom-up technique for pose estimation of arbitrary unknown objects (artic-

ulated, flexible, etc.) based on learning a direct mapping between features and poses in a learning stage, and combining the available data in the framework of the evidential reasoning. We showed how to use the EM algorithm for HMMs to build multi-Gaussian approximations of the feature spaces and direct feature-pose maps.

We adopted the evidential language to formalize and implement the information fusion, as the ToE makes no use of a-priori distributions, a very attractive feature in the context of model-free estimation. The ToE also provides tools to represent feature-pose maps through the notion of refining, and analyze incorrect inferences due to coarse approximations or ambiguities in the learnt model.

We chose to represent features as belief functions, also because of their relative simplicity. However, the use of Dempster's rule as fusion mechanism is implicitly based on the assumption that the pieces of evidence carried by the features are independent. This is reasonable in a model-free situation in which no a-priori knowledge of their relationships is available, and is often assumed in the literature. The approach has been tested in a challenging setup, concerning real video sequences with realistic non-static backgrounds. The experimental results support this assumption.

It would be interesting to understand what happens when we represent the uncertainty by means of some other class of imprecise probabilities, such as credal sets, coherent previsions, or the imprecise Dirichlet model. However, this well deserves a paper of its own, and will be the object of further research in the near future.

References

- [1] M. Bauer, *Approximation algorithms and decision making in the Dempster-Shafer theory of evidence—an empirical study*, International Journal of Approximate Reasoning **17** (1997), 217–237.
- [2] C. Bregler and J. Malik, *Tracking people with twists and exponential maps*, Proceedings of CVPR'98, Santa Barbara, CA, 1998.
- [3] B. R. Cobb and P. P. Shenoy, *A comparison of methods for transforming belief function models to probability models*, Proceedings of ECSQARU'2003, Aalborg, Denmark, July 2003, pp. 255–266.
- [4] F. Cuzzolin, *Algebraic structure of the families of compatible frames of discernment*, accepted for a Special Issue of the Annals of Mathematics and Artificial Intelligence (2005).
- [5] T. Denoeux and A. Ben Yaghlane, *Approximating the combination of belief functions using the fast Moebius transform in a coarsened frame*, International Journal of Approximate Reasoning **31(1-2)** (October 2002), 77–101.
- [6] D. M. Gavrila and L. S. Davis, *3D model-based tracking of humans in action: A multi-view approach*, Proceedings of CVPR'96, San Francisco, CA, 18-20 June 1996, pp. 73–80.
- [7] N. Howe, M. Leventon, and W. Freeman, *Bayesian reconstruction of 3D human motion from single-camera video*, Neural Information Processing Systems, Denver, Colorado, 1999.
- [8] T. Moeslund and E. Granum, *A survey of computer vision-based human motion capture*, Image and Vision Computing **81** (2001), 231–268.
- [9] L. Aggoun R. Elliot and J. Moore, *Hidden Markov models: estimation and control*, 1995.
- [10] J. M. Rehg and T. Kanade, *Model-based tracking of self-occluding articulated objects*, Proceedings of ICCV'95, 20-23 June 1995, pp. 618–623.
- [11] R. Rosales and S. Sclaroff, *Learning and synthesizing human body motion and posture*, Fourth Int. Conf. on Automatic Face and Gesture Recognition, Grenoble, France, March 2000.
- [12] G. Shafer, *A mathematical theory of evidence*, Princeton University Press, 1976.
- [13] Glenn Shafer, *Allocations of probability*, Annals of Probability **7:5** (1979), 827–839.
- [14] H. Sidenbladh and M.J. Black, *Learning the statistics of people in images and video*, IJCV **54** (2003), 189–209.
- [15] Philippe Smets, *Belief functions, Non-Standard Logics for Automated Reasoning* (Ph. Smets, A. Mamdani, D. Dubois, and H. Prade, eds.), Academic Press, London, 1988, pp. 253–286.
- [16] C. Sminchisescu and B. Triggs, *Covariance scaled sampling for monocular 3D body tracking*, Proceedings of CVPR'01, Hawaii, December 2001.
- [17] F. Voorbraak, *A computationally efficient approximation of Dempster-Shafer theory*, International Journal on Man-Machine Studies **30** (1989), 525–536.
- [18] A. Ben Yaghlane, T. Denoeux, and K. Mellouli, *Coarsening approximations of belief functions*, Proceedings of ECSQARU'2001 (S. Benferhat and P. Besnard, eds.), 2001, pp. 362–373.